Universities of Leeds, Sheffield and York
http://eprints.whiterose.ac.uk/

Terahertz Inverse Synthetic Aperture Radar Imaging Using Self-mixing Interferometry with a Quantum Cascade Laser

H. S. Lui,[1] T. Taimre,[2] Y. L. Lim,[1] K. Bertling,[1] P. Dean,[3] S. P. Khanna,[3] M. Lachab,[3] A. Valavanis,[3] D. Indjin,[3] E. H. Linfield,[3] A. G. Davies,[3] and A. D. Rakić[1, a)]

[1)]*School of Information Technology and Electrical Engineering, The University of Queensland, Brisbane, QLD 4072,*
Australia
[2)]*School of Mathematics and Physics, The University of Queensland, Brisbane, QLD 4072,*
Australia
[3)]*School of Electronic and Electrical Engineering, University of Leeds, Leeds LS2 9JT,*
United Kingdom

(Dated: 15 January 2014)

Imaging systems built around self-mixing interferometers have been successfully demonstrated at terahertz frequencies, exploiting the self-mixing process to probe the reflectivity of a remote target. In this letter, we propose a terahertz frequency synthetic aperture radar based on a quantum cascade laser which operates as a self-mixing interferometer, which addresses the need for higher resolution terahertz images. We demonstrate the system by imaging a standard resolution test target, achieving resolution beyond the diffraction limit.

Following the significant development of active terahertz (THz) frequency sources over the last two decades, extensive research effort has taken place to investigate imaging in the THz specral range.[1–6] THz pulsed imaging systems are the state-of-the-art solutions, and have been widely used in security screening, pharmaceutical, and biomedical applications.[2–5] With the recent demonstration of self-mixing (SM) in THz frequency quantum cascade lasers (QCLs),[7–9] however, imaging at THz frequencies through SM interferometry is a reality.[6,10,11] One common feature of these imaging systems, though, is that they form images through raster-scanning, illuminating a small portion of a remote target at a time. The resolution of the resultant image is therefore limited by the laser beam spot size, which is a function of the operating frequency and the diffraction limits of the optical system.

To overcome the spot-size-limited resolution, the measured scattered signals can be processed using synthetic aperture imaging techniques — synthetic aperture radar (SAR) and inverse SAR (ISAR).[12,13] These techniques are well known in the microwave radar literature and a considerable amount of work has been carried out at optical frequencies.[14,15] synthetic aperture imaging allows the creation of high resolution images by applying a coherent-sum process to measured scattered signals in such a way that the scattered signals are synthetically "back-propagated" to the target surface. In the last few years, synthetic aperture imaging techniques have been adapted to the THz spectral region. However, most of this work is applied at frequencies below 1 THz using microwave-based technologies (e.g. Ref. 16). In contrast, Danylov et al.[17] develop an experimentally-complex THz ISAR imaging system by phase-locking a THz QCL source to an optically-pumped molecular laser. Furthermore, an optical hetrodyning ISAR (employing a pair of acousto-optic deflectors) has been demonstrated,[18–20] capitalising on the high sensitivity and wide dynamic range of an optical feedback interferometer.

In this letter, we report a THz synthetic aperture imaging technique based on SM interferometry.[21–23] Using the SM effect, we demonstrate a THz SAR built around a directly modulated QCL. This reduces the complexity of the system; it removes the need for an external detector and modulator, but retains the high sensitivity and dynamic range inherent to coherent detection schemes.[18–20]

In SM interferometry, the radiation emitted from the laser interacts with the external target, is reflected, and partially re-injected into the laser cavity resulting in interference between the intra-cavity and reinjected fields ('self-mixing').[24,25] This perturbation to the intra-cavity field is manifested in the change in laser operating parameters, in particular in fluctuations in the voltage across the laser terminals, thus creating the SM signal.[8,11,26] Information about the external target (through its complex reflection coefficient) is embedded in the SM signal. Thus the reflected complex electric field can be detected coherently without an additional local oscillator or an external detector, thereby enabling extremely simple experimental configurations.

In our work, we combine this SM THz sensing system with SAR signal processing techniques to create THz images with spatial resolution well beyond the diffraction limit, as follows. When the spatial features of the imaged target are smaller than the laser beam spot size, (known as an extended target in the radar literature) the reflected electric field is a superposition of differential reflected fields from all points concurrently illuminated by the beam. This field can be expressed as[13]

$$E_{\boldsymbol{r}'}^{\text{Scattered}} = \int \rho(\boldsymbol{r}) e^{-jk2R(\boldsymbol{r},\boldsymbol{r}')+j\theta_{\text{R}}(\boldsymbol{r})} d\boldsymbol{r}, \qquad (1)$$

where $\boldsymbol{r}$ is the position on the target surface, $\boldsymbol{r}'$ corresponds to the position of the transmitter/receiver, k is the wavenumber, and $R(\boldsymbol{r}',\boldsymbol{r})$ corresponds to the distance between $\boldsymbol{r}$ and $\boldsymbol{r}'$. The term $\rho(\boldsymbol{r})$ represents the

———————
[a)]rakic@itee.uq.edu.au

square root of the radar cross section per differential volume. The factor of 2 appears as this is a mono-static setup — the transmitter and receiver are located at the same position. In conventional SAR and ISAR, the field given by (1) would have been the signal delivered to the receiver at the position $\boldsymbol{r}'$. In our SM configuration, this field is injected into the laser oscillator, where the nonlinear mixing of the reflected field with the intra-cavity field (of the local oscillator) occurs. By slowly modulating the laser frequency, this creates the nonlinear interferometric signal — our SM signal. The morphology of this signal is determined not only by the laser-target distance, but also the spatial distribution of the reflection coefficient across the illuminated spot on the target. The acquisition of a series of time-domain SM signals from successive, partially overlapping, spots on the target results in a set of signals containing information about this distribution. From each of these SM waveforms we extract the corresponding "effective" (aggregate) complex reflection coefficient of the illuminated part of the target. Based on the known laser-target distance and the extracted effective complex reflection coefficient we calculate the relative magnitude and the phase of the back-scattered electric field given by (1) just in front of the exit mirror of the QCL. We repeat this procedure at each relative position of the laser-target assembly, after lateral translation of the target.

At this stage of the process, an array of scattered complex electric field values corresponding to each spatial location of the transceiver (the exit facet of the QCL) relative to the target has been obtained. We next pass this array of complex numbers to our ISAR algorithm, which is used to recover the actual (high-resolution) spatial dependence of the complex reflectivity (or in general the radar cross section) across the target surface.

Our ISAR algorithm is a single-frequency implementation of a conventional matched-filter.[27,28] The essence of this well-known algorithm resides in using all measured scattered electric fields to calculate the strength of reflection from any given point on the target surface (known as a scattering center in the radar literature). We infer the reflection coefficient at a particular point on the target as the superposition (coherent sum) of the electric field array components back-projected to that point (that is, multiplied by $e^{+jk2R(\boldsymbol{r},\boldsymbol{r}')}$). This results in an array of complex numbers whose magnitudes are proportional to the reflection coefficient of the target, which we interpret as the reconstructed high-resolution image of the target.

We present experimental results using a target which is the negative of a (high resolution) 1951 US air force resolution test chart consisting of chromium deposited on soda lime glass. Figure 1 shows the schematic diagram of the experimental apparatus. The THz QCL (operating at 2.59 THz) consisted of a 11.6 µm thick GaAs/AlGaAs bound-to-continuum active region that was processed into a semi-insulating surface-plasmon ridge waveguide with dimensions 1.78 mm × 140 µm. The QCL was mounted onto the cold finger of a continuous-flow cryo-
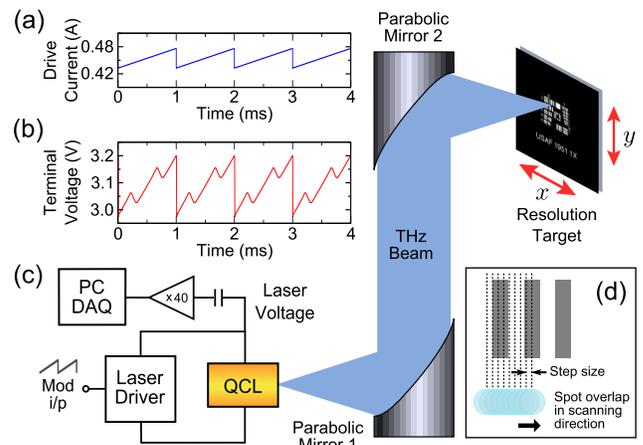

FIG. 1. Schematic diagram of the experimental apparatus used for target measurements. (a) Current stimulus signal; the current range was selected to sweep the laser frequency through three external cavity resonances in the region where the laser was most sensitive to optical feedback. (b) Corresponding SM voltage signal measured across the laser terminals after 40 × gain (28dB) with a static target. For illustrative purposes, the magnitude of the SM signal has been increased ten-fold. The voltage signal shown is typical for this experimental arrangement. (c) The amplified SM voltage is acquired using a computer-based data acquisition card (PC DAQ). A pair of off-axis parabolic mirrors focusses the beam onto the target, mounted on a computer-controlled translation stage. (d) Measurements are performed in a raster-scanning fashion. The target is moved laterally such that different portions of it are illuminated at each step. The step size of each lateral movement is smaller than the spot size resulting in overlapping area between each measurement.

stat fitted with a polyethylene window and operated in continuous wave mode at a heat sink temperature of 15 K. Radiation from the QCL was collimated using a 2 inch diameter, 4 inch focal length ($f/2$) off-axis parabolic reflector and focussed onto the target using a second identical mirror. The resulting beam spot in the focus was found to be approximately circular with a $1/e^2$ diameter of 200 µm. The total optical path between source and target was 568.2 mm through an ambient (unpurged) atmosphere. The laser was driven by a current source at $I_{dc} = 0.43$ A, slightly above the threshold ($I_{th} = 0.40$ A), where the sensitivity to optical feedback is at a maximum.[10] A modulating saw-tooth current signal (50 mA peak-to-peak amplitude, Fig. 1(a)) was superimposed on the dc current leading to a linear frequency sweep of 600 MHz. SM voltage waveforms are measured across the laser terminals after $40\times$ gain has been applied (Fig. 1(b)). For image acquisition, the target was scanned linearly in one dimension using a motorised translation stage, and the recorded SM voltage signal was the average of 128 traces.

The target used consists of a series of line pairs (alternating between chromium and soda-lime glass) with variable spatial frequency. Two parts of the target (groups)
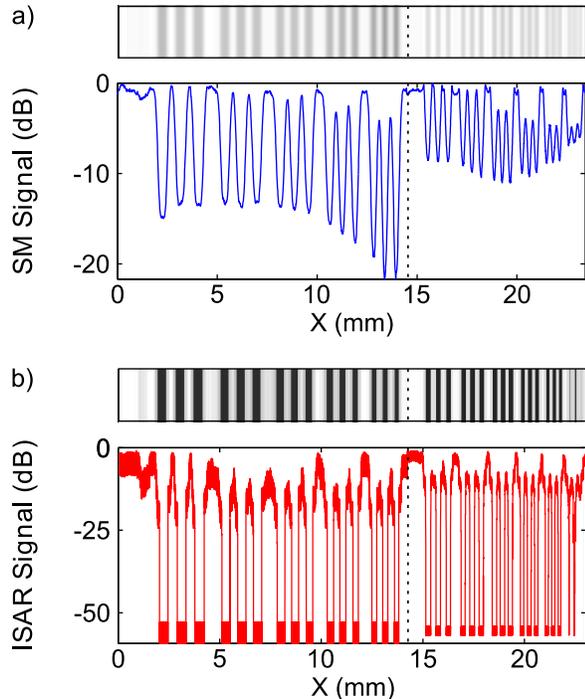
FIG. 2. Imaging results: (a) unprocessed SM image acquired through raster scanning, and (b) processed ISAR image. The dotted vertical line separates the two scanned portions of the target. The horizontal axis in (a) corresponds to the relative target measurement position in the one-dimensional raster scan, while that in (b) corresponds to the position of the reconstructed scattering profile at the target surface.
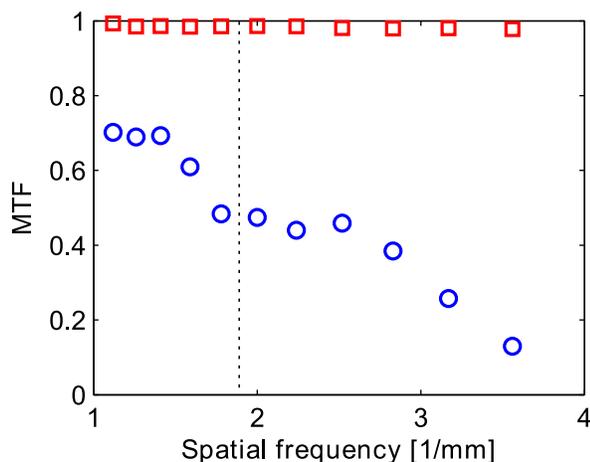

FIG. 3. Modulation transfer function of the unprocessed (circles) and processed (squares) imaging modalities. The dotted vertical line separates the two scanned portions of the target.

were scanned (see Fig. 2). The first group (to the left of the broken line in Figs. 2 and 3) consisted of five elements containing three line pairs, varying in spatial frequency from 1.12 to 1.78 line pairs per millimetre. This group was rastered with a 10 µm step. The second group consisted of six elements containing three line pairs, varying in spatial frequency from 2.00 to 3.56 line pairs per millimetre, and was rastered with a 5 µm step.

The root-mean-square of the SM signal as a function of position (along the x axis) is shown in Fig. 2(a). The upper panel of Fig. 2(a) shows that the usual unprocessed raster scanning approach is able to resolve all the bars. However, the contrast decreases as the spatial frequency increases (to the right). The maximum change in signal across the target surface, which corresponds to the reflected signal from chromium relative to that from soda lime glass, is around 15dB.

The result of reconstructing the scattering profile of the target is shown in Fig. 2(b), using a spatial pitch of 1 µm when applying the matched filter. It is apparent that the bars are more sharply resolved, particularly as the bar thickness decreases, with about 50 dB change in signal level observed across this portion of the target.

The modulation transfer function (MTF), which is a measure of how faithfully an optical system reproduces details of an object in the image, is used to quantify the performance of the image reconstruction process. Mathematically it is given by $(I_{\max} - I_{\min})/(I_{\max} + I_{\min})$, where $I_{\max}$ and $I_{\min}$ are the maximum and minimum intensities in the image respectively. An MTF value of 1 indicates that the image is perfectly resolved. The MTFs for both the unprocessed and ISAR approaches are shown in Fig. 3; it is evident that the synthetic aperture signal processing significantly improves the contrast and spatial resolution of the resultant images.

In summary, we have demonstrated a synthetic aperture imaging approach based on self-mixing interferometry. We have been able to extract the corresponding "radar signal" from the measured self-mixing signals. A matched filter is then applied, resulting in a significant improvement of contrast and spatial resolution in the processed image. The developed synthetic-aperture self-mixing imaging technique is able to resolve target features that are smaller than the spot size, and so is well suited to high resolution, high-sensitivity imaging at THz frequencies without the need for an external detector.

[1] B. Hu and M. Nuss, Opt. lett. **20**, 1716 (1995).

[2] V. P. Wallace, E. MacPherson, J. A. Zeitler, and C. Reid, J. Opt. Soc. Am. A **25**, 6 (2008).

[3] A. Fitzgerald, E. Berry, N. Zinovev, G. Walker, M. Smith, and J. Chamberlain, Phys. Med. Biol. **47**, R67 (2002).

[4] V. P. Wallace, P. F. Taday, A. J. Fitzgerald, R. M. Woodward, J. Cluff, R. J. Pye, and D. D. Arnone, Farad. Discuss. **126**, 255 (2004).

[5] A. J. Fitzgerald, B. E. Cole, and P. F. Taday, J. Pharm. Sci. **94**, 177 (2005).

[6] P. Dean, A. Valavanis, J. Keeley, K. Bertling, Y. Leng Lim, R. Al-hathlool, S. Chowdhury, T. Taimre, L. H. Li, D. Indjin, S. J. Wilson, A. D. Rakić, E. H. Linfield, and A. Giles Davies, Appl. Phys. Lett. **103**, 181112.1 (2013).

[7] R. P. Green, J. H. Xu, L. Mahler, A. Tredicucci, F. Beltram, G. Giuliani, H. E. Beere, and D. A. Ritchie, Appl. Phys. Lett. **92**, 071106 (2008).

[8] Y. L. Lim, P. Dean, M. Nikolić, R. Kliese, S. P. Khanna, M. Lachab, A. Valavanis, D. Indjin, Z. Ikonić, P. Harrison, E. H. Linfield, A. G. Davies, S. J. Wilson, and A. D. Rakić, Appl. Phys. Lett. **99**, 081108 (2011).

[9] F. Mezzapesa, L. Columbo, M. Brambilla, M. Dabbicco, S. Borri, M. Vitiello, H. Beere, D. Ritchie, and G. Scamarcio, Opt. Express **21**, 13748 (2013).

[10] P. Dean, A. Valavanis, Y. L. Lim, S. P. Khanna, M. Lachab, R. Kliese, M. Nikolić, Z. Ikonić, D. Indjin, P. Harrison, A. D. Rakić, E. H. Linfield, and A. G. Davies, Opt. Lett. **36**, 2587 (2011).

[11] A. D. Rakić, T. Taimre, K. Bertling, Y. L. Lim, P. Dean, D. Indjin, Z. Ikonić, P. Harrison, A. Valavanis, S. P. Khanna, M. Lachab, S. J. Wilson, E. H. Linfield, and A. G. Davies, Opt. Express **21**, 22194 (2013).

[12] D. L. Mensa, *High Resolution Radar Cross-Section Imaging* (Artech House, 1991).

[13] R. J. Sullivan, *Radar Foundations for Imaging and Advanced Concepts* (Scitech Publishing, 2004).

[14] S. Marcus, B. D. Colella, T. J. Green Jr, *et al.*, Appl. Opt. **33**, 960 (1994).

[15] V. Molebny, G. Kamermanb, and O. Steinvallc, in *Proc. of SPIE*, Vol. 7835 (2010) pp. 783502–1.

[16] J. Moll, P. Schops, and V. Krozer, IEEE Trans. Terahertz Sci. Technol. **2**, 432 (2012).

[17] A. A. Danylov, T. M. Goyette, J. Waldman, M. J. Coulombe, A. J. Gatesman, R. H. Giles, X. Qian, N. Chandrayan, S. Van-gala, K. Termkoa, *et al.*, Opt. Express **18**, 16264 (2010).

[18] A. Witomski, E. Lacot, O. Hugon, and O. Jacquin, Optics letters **31**, 3031 (2006).

[19] A. Witomski, E. Lacot, O. Hugon, and O. Jacquin, Applied optics **47**, 860 (2008).

[20] W. Glastre, E. Lacot, O. Jacquin, O. Hugon, and H. G. De Chatellus, JOSA A **29**, 476 (2012).

[21] R. Lang and K. Kobayashi, IEEE J. Quantum Electron. **QE-16**, 347 (1980).

[22] G. Giuliani, M. Norgia, S. Donati, and T. Bosch, J. Opt. A, Pure Appl. Opt. **4**, S283 (2002).

[23] S. Donati, Laser Photon. Rev. **6**, 393 (2012).

[24] D. M. Kane and K. A. Shore, *Unlocking dynamical diversity: optical feedback effects on semiconductor lasers* (Wiley, 2005).

[25] S. Donati, *Electro-Optical Instrumentation, Sensing and Measuring with Lasers* (Prentice Hall, Upper Saddle River, NJ, 2004).

[26] Y. L. Lim, K. Bertling, P. Rio, J. R. Tucker, and A. D. Rakić, in *Proc. SPIE Int. Soc. Opt. Eng.*, Vol. 6038 (2006) pp. 60381O–10.

[27] A. Gunawardena and D. Longstaff, in *Radar Conference, 1995., Record of the IEEE 1995 International* (1995) pp. 239–243.

[28] C. Ozdemir, *Inverse synthetic aperture radar imaging with MAT-LAB algorithms* (John Wiley, Hoboken, NJ, 2012).